Nano Energy 77 (2020) 105034

Contents lists available at ScienceDirect

Nano Energy

journal homepage: http://www.elsevier.com/locate/nanoen

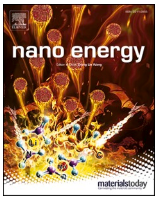

Surface engineering of $LiNi_{0.8}Mn_{0.1}Co_{0.1}O_2$ towards boosting lithium storage: Bimetallic oxides versus monometallic oxides

Quan Xu [a,b], Xifei Li [a,b,**], Hirbod Maleki Kheimeh Sari [a,b], Wenbin Li [a,b], Wen Liu [a,b], Youchen Hao [a,b], Jian Qin [a,b], Bin Cao [a,b], Wei Xiao [a,b], Yue Xu [a,b], Yuan Wei [a,b], Liang Kou [c], Zhanyuan Tian [c], Le Shao [c], Cheng Zhang [c], Xueliang Sun [d,a,b,*]

[a] *Xi'an Key Laboratory of New Energy Materials and Devices, Institute of Advanced Electrochemical Energy & School of Materials Science and Engineering, Xi'an University of Technology, Xi'an, Shaanxi, 710048, China*
[b] *Shaanxi International Joint Research Center of Surface Technology for Energy Storage Materials, Xi'an, Shaanxi, 710048, China*
[c] *Shaanxi Coal Chem. Ind. Technol. Res. Inst. Co. Ltd., Xian, Shaanxi, 710070, China*
[d] *Department of Mechanical and Materials Engineering, University of Western Ontario, London, ON, N6A 5B9, Canada*

ARTICLE INFO

Keywords:
Bimetallic oxide
Multifunctional coating
NCM811
Lithium ion batteries

ABSTRACT

Although conventional monometallic oxide coating on lithium nickel cobalt manganese oxide (NCM) cathode materials has been extensively investigated, there are still many issues, such as low electrical conductivity, poor mechanical properties and inferior chemical stability, that need to be addressed. Indeed, because of the single nature of monometallic oxides, it is difficult to achieve the synergistic effect of various properties. In this work, $NiCo_2O_4$ were rationally grown on the surface of commercial $LiNi_{0.8}Mn_{0.1}Co_{0.1}O_2$ (NCM811) to obtain a bimetallic oxide coated NCM811 as cathode material for Lithium ion batteries (LIBs). This cleverly designed coating with a higher electronic and ionic conductivity, better bulk modulus, and an outstanding interfacial stability, could improve the capacity retention to 90.97% after 200 cycles at 100 mA g^{-1} and enhance the initial coulombic efficiency (CE) to 82.92%. The electrochemical characterization further clarifies the indisputable benefits of $NiCo_2O_4$ coating to enhancement of the cathode performance. Moreover, the theoretical calculations provide more explanations in three aspects, including mechanical stability, chemical stability and electrical properties, confirming the superiority of $NiCo_2O_4$ bimetallic oxide coating with multiple properties over the monometallic one. More importantly, this study has profound implications in the design of bimetallic and polymetallic oxide coatings for electrode materials, and even other bimetallic coatings, such as sulfides and selenides, in the future.

1. Introduction

The energy crisis is becoming a globally daunting issue due to the increasing demand for energy and the depletion of traditional fossil fuels, leading to a destructive impact on the environment. In order to solve this contradiction, great efforts have been made to develop green and sustainable energy sources, among which electrochemical storage and conversion technologies have proven to be very effective. Since the commercialization in 1991, LIBs have gradually shown great advantages in their application, occupying the largest market share among the rechargeable batteries. Because of the high energy, long cycle-life and other advantages, they have been widely employed in electric vehicles, grid energy storage, and electronic devices [1,2]. The performance of full batteries strongly depends on cathode materials, which are more difficult to develop and more expensive to produce than the widely used graphite or other more advanced anode materials [3,4]. Accordingly, Ni-rich NCM ($LiNi_xMn_yCo_{1-x-y}O_2$, $0.6 < x < 1$, $0 < y < 0.2$) originated from partial cation substitution of Ni atoms in $LiNiO_2$, is considered as a promising candidate because of its large capacity and low manufacturing cost compared to conventional $LiFePO_4$ and $LiCoO_2$ cathodes [5–8]. However, Ni-rich NCM cathodes suffer from various types of electrochemical degradation phenomena such as cation

---

* Corresponding author. Department of Mechanical and Materials Engineering, University of Western Ontario, London, ON, N6A 5B9, Canada.
** Corresponding author. Xi'an Key Laboratory of New Energy Materials and Devices, Institute of Advanced Electrochemical Energy & School of Materials Science and Engineering, Xi'an University of Technology, Xi'an, Shaanxi, 710048, China.
E-mail addresses: xfli2011@hotmail.com (X. Li), xsun@eng.uwo.ca (X. Sun).

https://doi.org/10.1016/j.nanoen.2020.105034
Received 20 March 2020; Received in revised form 28 May 2020; Accepted 29 May 2020

disorder, phase transformation, and side reaction at the electrolyte-electrode interface, which are significant barriers for their further large-scale application and commercialization [8–12].

Surface coating is an efficient method to alleviate the degradation behaviors in Ni-rich NCMs by providing a physical barrier on the surface, which prevents the direct contact between the electrode and electrolyte [13]. For example, metal oxides such as Al_2O_3 [14,15], Co_3O_4 [16,17], SiO_2 [18], TiO_2 [19], ZnO [20] and WO_3 [21] are demonstrated to be successfully effective in improving the capacity retention of the layered cathode materials during electrochemical cycling. Metal phosphates [22], fluorides [23] and conducting polymers [24] are also popular and broadly applied as coating materials. In addition, for boosting the Li^+ diffusion at the interface, Li-containing materials such as $LiAlO_2$ [25], Li_2MnO_3 [26,27], Li_2TiO_3 [28], Li_2ZrO_3 [29] and $LiNbO_3$ [30] have been investigated, exhibiting great rate capability and improved cycle-life. Among the various coating materials, oxides are the most widely studied and applied in both academia and industry. In spite of their great functionality, the aforementioned approaches have several drawbacks because the coating materials typically result in a lower initial capacity compared to the uncoated electrodes [31]. Another critical concern is the poor electronic and ionic conductivities of some coating layers, which may have a negative effect on the electrochemical kinetics of NCMs. Hence, the coating layer as a physical barrier with positive effects can simultaneously act as an electrochemical obstacle with negative effects. Hence, designing a multifunctional coating with both excellent physical and chemical properties is essential to achieve more efficient batteries.

Based on the critical aspects of surface coatings discussed above, an ideal coating material should possess the following functionalities: 1) excellent mechanical properties, buffering volume expansion during cycling; 2) high electronic and ionic conductivity, improving kinetics of extraction/insertion of Li^+; 3) perfect chemical stability, reducing the erosion of cathode by electrolyte. Hence, in this work, a bimetallic oxide (i.e., $NiCo_2O_4$) as the coating layer for NCM811 is designed and compared with the monometallic oxides (i.e., NiO and Co_3O_4) and their mixture in order to achieve the above-mentioned modification effects and ameliorate the electrochemical performance of the cathode material. It also displays a high initial CE of 82.92% and a superb capacity retention of 90.97% after 200 cycles at 100 mA g^{-1}. Indeed, the theoretical calculations further verify the superior performance of the bimetallic oxide coating.

2. Experimental

2.1. Material synthesis

Commercial NCM811 coated with $NiCo_2O_4$ was synthesized by a simple solvothermal method. In particular, 0.61 mg $Ni(NO_3)_2{\cdot}6H_2O$, 1.21 mg $Co(NO_3)_2{\cdot}6H_2O$ and 0.29 mg HMTA, as a complexing agent, were dissolved into 40 mL ethanol, then transferred into a Teflon-lined stainless-steel autoclave which was sealed and kept at 120 °C for 12 h, and then cooled down to room temperature. The as-obtained black product was washed with ethanol several times, followed by drying at 90 °C for 1 h. The obtained black powder was transferred into a tube furnace and heated at 400 °C for 2 h with a heating rate of 1 °C/min in the N_2 flow, and then naturally cooled down to room temperature to obtain the $NiCo_2O_4$ coated NCM811 (denoted as Ni&Co-NCM), ultimately. For comparison, other coated samples were synthesized by a similar method. Nickel oxide was coated on NCM811 (denoted as Ni-NCM) without the additive of $Co(NO_3)_2{\cdot}6H_2O$. Cobalt oxide was coated on NCM811 (denoted as Co-NCM) without the additive of $Ni(NO_3)_2{\cdot}6H_2O$. Complexing agent, HMTA, was not involved to co-coated nickel oxide and cobalt oxide on NCM811 (denoted as Ni/Co-NCM). To verify the phase of coating layer, we repeated the aforementioned processes without NCM to obtain $NiCo_2O_4$, NiO, Co_3O_4 and the mixture of NiO and Co_3O_4.

2.2. Material characterization

The phase of each sample was identified by X-ray Diffraction (XRD, SHIMADZU XRD-7000). The morphologies and microstructures were analyzed by field emission scanning electron microscopy (FESEM, JSM-6700F) and double spherical aberration correction field emission transmission electron microscope (ACTEM, FEI Themis Z). The composition of materials and valence state of elements were indicated by X-ray photoelectron spectroscopy (XPS, Thermo Fisher ESCALAB Xi^+).

2.3. Electrochemical characterization

LIR2032 coin cells were assembled to study the electrochemical performance. NCM811, super P and PVDF with a weight ratio of 8:1:1 on aluminum foil was used as the working electrode, and lithium foil was used as the counter electrode and reference electrode, and 1.0 M $LiPF_6$ in ethylene carbonate (EC), dimethyl carbonate (DMC), and ethylene methyl carbonate (EMC) (1:1:1 Vol%) with 10.0% fluoroethylene carbonate (FEC) and 2.0% vinylene carbonate (VC) was used as the electrolyte. Electrochemical performance was tested by a galvanostatic charge-discharge system (Neware) between 3.0 V and 4.5 V (vs. Li/Li^+) at room temperature. Cyclic voltammetry (CV) curves and electrochemical impedance spectroscopy (EIS) were carried out on a Princeton Applied Research VersaSTAT 4 electrochemical workstation.

2.4. Theoretical calculation

First principle density functional theory (DFT) calculations have been performed for atomic configuration optimization and energy calculations. For all calculations, the Perdew-Burke-Ernzerhof (PBE) function and projector augmented-wave (PAW) [32,33] method are adopted using the Vienna Ab initio Simulation Package (VASP). In each calculation, an energy cut-off of 520 eV were adopted with an energy difference of less than 0.01 eV. When performing the structural optimization, the system is regarded as converged when the force per atom is less than 0.01 eV $Å^{-1}$. Moreover, regarding the co-coating NiO and Co_3O_4, which is a physical mixture, the following calculations assume that the physical properties of this coating depends on the average effect of NiO and Co_3O_4.

3. Results and discussion

According to Fig. 1a, the XRD patterns of the pristine and coated NCM with different coatings all show the same diffraction peaks, perfectly matched $LiNiO_2$ (PDF # 89–3601), which is a typical layered structure transition metal (TM) oxide [34]. It indicates that the phases of NCM after coating via solvothermal method have not been changed, and perfectly maintained its original layered form. To confirm the phases of coating layers, the XRD test was conducted for each of them before coating the NCM, as illustrated in Fig. 1b–e, which are respectively identical to $NiCo_2O_4$ (PDF # 20–0781), NiO (PDF # 78–0423), Co_3O_4 (PDF # 43–1003) and NiO/Co_3O_4 [35–37].

To directly characterize the NCM powder, SEM and TEM tests were carried out. Fig. 2a shows the morphology of the pristine NCM secondary particles, which are composed of single crystal primary particles. The high magnification SEM image in Fig. 2b and TEM image in Fig. 2c show the smooth surface of NCM while the high magnification TEM image in Fig. 2d can reveal more details about its morphology. The spacing of the lattice fringe in the region marked with the red square is 0.204 nm, corresponding to the (104) crystal plane of NCM. The fast Fourier transform (FFT) image embedded in Fig. 2d also indicates the good crystallinity of the pristine NCM. Moreover, the detailed morphology and structure of Ni&Co-NCM is depicted in Fig. 2e–h. The presence of a conformal coating layer with a rough and fuzzy surface is detectable in Fig. 2e and f. According to the TEM image in Fig. 2g the thickness of the coating layer is about 2 nm. Meanwhile, the lattice

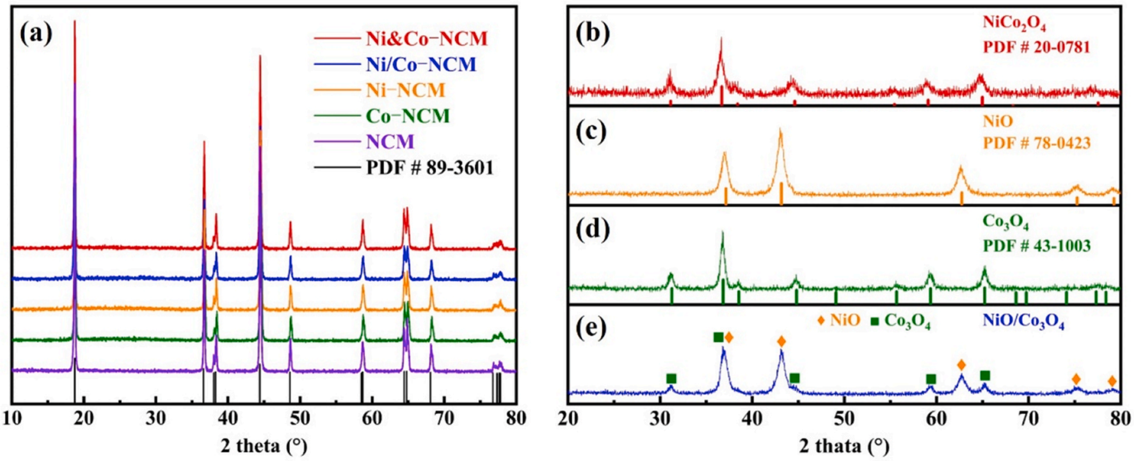

Fig. 1. XRD patterns of the material: (a) Pristine NCM and the NCM coated with different coatings; (b–e) four different coatings, including $NiCo_2O_4$, NiO, Co_3O_4 and NiO/Co_3O_4, respectively.

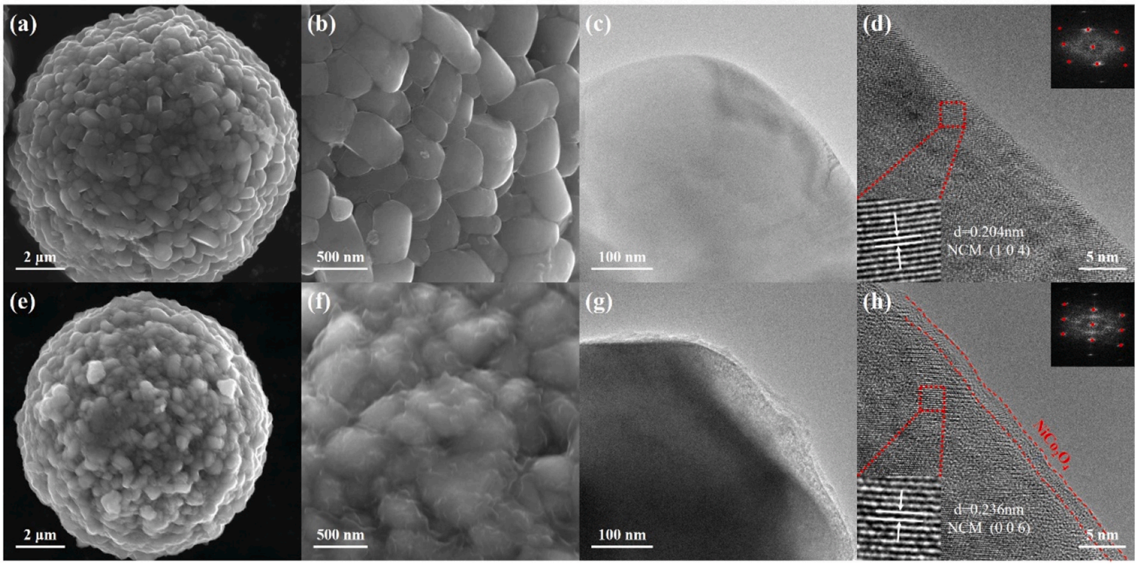

Fig. 2. (a, b) SEM and (c, d) TEM images of NCM; (e, f) SEM and (g, h) TEM images of Ni&Co-NCM.

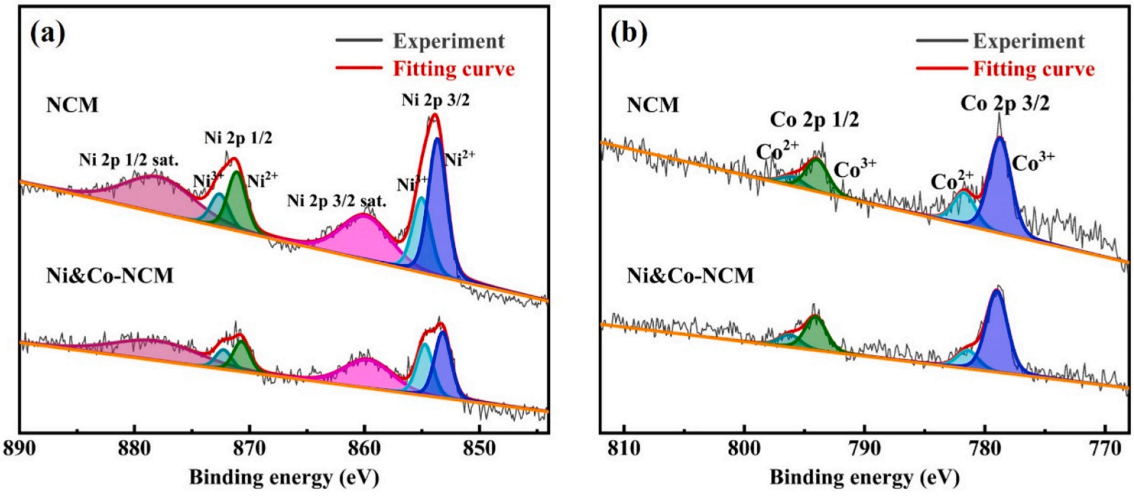

Fig. 3. High resolution XPS spectra of (a) Ni 2p and (b) Co 2p for the pristine NCM and Ni&Co-NCM.

fringe and FFT image in Fig. 2h indicate that the original structure and crystallinity of NCM have remained intact after the coating process. Therefore, combined with the XRD result in Fig. 1b, it can be concluded that the $NiCo_2O_4$ coated NCM has been successfully synthesized. Indeed, more detailed information and images of the other samples is shown in Figs. S1 and S2, and this conclusion can also be obtained from the lattice fringes of each coating layer. As expected, different thin coating layers were formed on the surface of the other three coated NCM samples, among which the coating layer of Ni/Co-NCM is not conformal, which may be due to the different nucleation and growth rates of NiO and Co_3O_4 on the surface.

XPS test was also conducted before assembling the coin cells to investigate the materials composition and the elements valence states. The peaks corresponding to Li 1s, C 1s, O 1s, Mn 2p, Co 2p and Ni 2p were discovered as shown in Fig. S3. More details are shown in Fig. 3 and Fig. S4, which display Ni 2p spectra and Co 2p spectra for all samples. The valence state of Ni 2p is a mix of Ni^{2+} and Ni^{3+}. Particularly, taking the pristine NCM as an example (Fig. 3a), the Ni 2p 1/2 peak at about 871.3 eV and Ni 2p 3/2 peak at 853.9 eV can be split into Ni^{2+} (853.66 eV and 871.11 eV) and Ni^{3+} (855.03 eV and 872.59 eV). Indeed, the Co 2p 1/2 and Co 2p 3/2 peaks at about 794.1 eV and 778.8 eV in Fig. 3b, respectively, can be divided into Co^{2+} (781.71 eV and 796.00 eV) and Co^{3+} (778.73 eV and 793.96 eV) [15,24,27,28,35,38–40].

Table 1 lists the ratios of different Ni and Co valance states for each coating on the surface of NCM particles. Evidently, the ratio of Ni^{3+} has increased after NiO coating, while the proportion of Co cations are almost constant. Similarly, after Co_3O_4 coating or co-coating of NiO and Co_3O_4, Co^{3+} ratio has increased, but the proportion of Ni cations have remained almost unchanged. When it comes to $NiCo_2O_4$ coating, both ratios of Ni^{3+} and Co^{3+} increase by a certain amount, which indirectly verifies the successful formation of different oxides in the coating layer. Different metal elements have different binding energies with oxygen, yielding different reactions towards accommodating volume expansion during cycling and resisting HF corrosion, which both are important factors affecting the cycle-life of a battery. Later in this study, more and stronger evidence are presented by theoretical calculations to confirm the formation of metallic oxides in the coating layer.

To evaluate the performance of Ni&Co-NCM as the cathode material for LIBs, the charge-discharge test, displaying several cycles of Ni&Co-NCM at a current density of 100 mA g^{-1} was carried out (Fig. 4a). The charging/discharging diagram maintains its original form even after 200 cycles, which is indicative of an excellent cycling stability. In Fig. 4b and Fig. S5, which show the charge-discharge curves at the first and 200th cycles, all samples show a similar pattern, indicating that coating does not change the electrochemical reaction of the materials. Indeed, the CE of the first cycle for the coated samples, particularly for Ni&Co-NCM which is up to 82.92%, have significantly improved compared to that for the pristine NCM. It is also worth noting that the ohmic polarization (ΔE_{Ω}) of samples with or without coating have changed, manifesting the potential difference between the charge termination and discharge initiation voltages. During the test, the standing time is set to 1 min to ensure that the lithium ion diffusion of different samples within the resting between charge and discharge process is of comparableness. Even though the ΔE_{Ω} of the coating samples are larger than that of the pristine NCM at the first cycle, the growth of the ΔE_{Ω} is smaller after 200 cycles. Notably, at the beginning of the cycles, Ni&Co-NCM may not show some advantages over the pristine NCM, even with a decrease in capacity. The coating layer formed on the NCM surface is inactive with a lower conductivity of lithium ion compared with the pristine NCM, resulting in the reduction of discharge capacity. But upon cycling, benefiting from the protection effect, the coating layer reflected obvious positive impact on NCM stability. The results distinctly demonstrate the superior cycle performance of the coated samples, and particularly Ni&Co-NCM with a capacity retention up to 90.97%, as shown in Fig. 4c. Interestingly, as the cycling continues, benefits of the coating layer becomes more pronounced. To further confirm the coating effect on cycling performance, the morphologies of the electrodes after 200 cycles were tested. As shown in Fig. S6, some microcracks obviously appeared on the surface of the pristine NCM after 200 cycles, and some particles were even broken. By contrast, Ni&Co-NCM may remain intact spherical particles without obvious cracks. In addition, the XRD results after 200 cycles are shown in Fig. S7. The peaks located at around 38°, 44°, 65° and 78° originate from the current collector in the electrodes. Compared with samples before cycling, the samples after cycles may maintain the original phase.

Table 1
The ratio of different valence states of Ni and Co on the surface of the five samples.

	Ni^{2+}	Ni^{3+}	Co^{3+}	Co^{2+}
NCM	64.76%	35.24%	74.38%	25.62%
Ni-NCM	57.98%	42.02%	75.49%	24.51%
Co-NCM	62.28%	37.72%	85.61%	14.40%
Ni/Co-NCM	62.49%	37.51%	83.33%	16.67%
Ni&Co-NCM	56.13%	43.87%	84.57%	18.43%

According to Fig. 4d and Fig. S8, compared to the pristine NCM, Ni&Co-NCM keeps more stable oxidation and reduction peaks [34,41]. The value of the potential difference between oxidation peaks at the first and the fifth cycles (ΔE_E) is in a direct relationship with side reaction and electrochemical polarization during the initial several cycles [25,42]. The ΔE_E values are listed in Table 2. Evidently, the ΔE_E of Ni-NCM is larger than that of the pristine NCM while those of the other three coated samples are smaller. During the charge-discharge process, extraction and insertion of Li^+ in NCM particles lead to a change in the valence of Ni and increase the chance of Li–Ni cation mixing, which results in the formation of rock-salt phase NiO on the surface and more side reactions [39]. It is worth mentioning that the conductivity of Ni-NCM is very low owing to evolution of the rock-salt phase NiO coating on the surface. Oppositely, the electrical conductivity of the other three coatings are increased due to the addition of Co which can reduce the influence of electrochemical polarization. This is also supported by the change of H2→H3 phase transition peaks, shown in Fig. S9. At the first cycle of CV, the H2→H3 phase transition peaks of Ni&Co-NCM, Ni-NCM, Co-NCM, Ni/Co-NCM and NCM seem similar, and their difference is obvious at the sequent cycles, especially for Ni/Co-NCM. As the results in TEM test, the different nucleation and growth rates of NiO and Co_3O_4 on the surface lead to the coating layer of Ni/Co-NCM is not conformal. Due to uneven coating layer of Ni/Co-NCM, uncoated area may be more prone to surface reconstruction in comparison to the coated areas, leading to a decrease of CV peak at around 4.2 V for the H2→H3 phase transition. Fig. 4e and Fig. S10 illustrate the CV curves at various scan rates, and the relationship of the peak current (i_p) and the square root of scan rate ($v^{1/2}$) are depicted in Fig. 4f to acquire the lithium-ion diffusion rate (D_{Li^+}) using the Randles–Sevcik equation [43,44]:

$$i_p = 2.69\times\ 10^5\ n^{3/2}\ A\ C_0\ D_{Li^+}^{1/2} v^{1/2}$$

where n is the number of electrons in redox reaction; A is the geometric area of electrode (cm^2); C_0 is the molarity of lithium ions (mol cm^{-3}), D_{Li^+} is the diffusion rate of lithium ions, and v is the potential scan rate (V s^{-1}). The D_{Li^+} in all samples are of the same order of magnitude, as listed in Table 2, indicating that coating modification has no negative effect on ion conduction. This is because the thickness and ratio of the coating layers are very small relative to the bulk phase material, thus the diffusion coefficient of lithium ions in the cathodes hardly changes.

EIS has been considered as an effective method to determine the ohmic resistance (R_s), surface film resistance (R_f) and charge transfer resistance (R_{ct}) [45,46]. Before testing, the cells were charged to 3.75 V at 100 mA g^{-1} after various cycles. The Nyquist plots of the pristine NCM

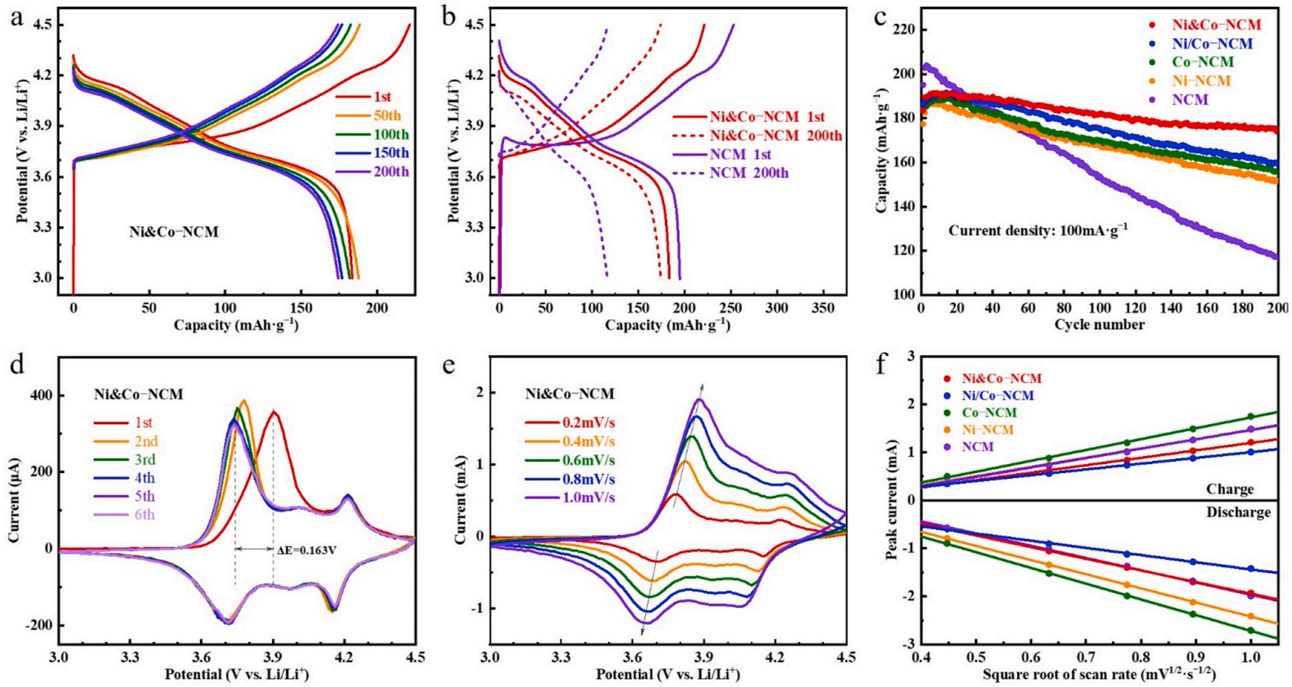

Fig. 4. (a) Charge-discharge curves of different cycles of Ni&Co-NCM; (b) The first and 200th charge-discharge curves of the pristine NCM and Ni&Co-NCM; (c) Cycle performance of the five samples; CV curves of (d) Ni&Co-NCM at the scan rate of 0.1 mV s^{-1}, and (e) Ni&Co-NCM at various scan rates; (f) Relationship of the peak current (i_p) and the square root of scan rate ($v^{1/2}$).

Table 2
Values of ΔE_E, ΔE_Ω, initial coulombic efficiencies, capacity retention and lithium-ion diffusion coefficients of the five samples.

		NCM	Ni-NCM	Co-NCM	Ni/Co-NCM	Ni&Co-NCM
Initial CE		76.99%	69.60%	76.66%	78.10%	82.92%
ΔE_Ω (V)	1st	0.095	0.207	0.169	0.196	0.182
	200th	0.299	0.327	0.283	0.315	0.272
Capacity retention		57.41%	80.75%	82.38%	83.03%	90.97%
ΔE_E (V)		0.229	0.255	0.194	0.153	0.163
D_{Li^+} (cm^2 s^{-1})	extraction	1.7×10^{-11}	1.6×10^{-11}	2.3×10^{-11}	0.6×10^{-11}	1.1×10^{-11}
	insertion	2.9×10^{-11}	3.9×10^{-11}	4.8×10^{-11}	1.0×10^{-11}	2.6×10^{-11}

and Ni&Co-NCM distinctively follow two different models, and consequently different equivalent circuits. The former can fit in three arcs after a few cycles, indicating the presence of three interfaces between solid and liquid phases, while the latter can merely fit in two arcs after 200 cycles [47] (Fig. 5a and b). It suggests that the pristine NCM forms one more interface during cycling because the number of arcs represent the number of interfaces. This signifies the positive effect of the coating layer on protecting the pristine NCM through cycling. However, not all the coatings are beneficial in this regard; for instance, NiO coating and NiO/Co_3O_4 co-coating increase the resistance to a certain extent. Compared to R_{ct}, R_s and R_f account for a very small percentage of the total resistance during cycling. Therefore, the continuous increase of the R_{ct} is considered to be the leading reason for capacity decay. The R_{ct} values of the five samples are listed in the 3D column chart in Fig. 5c. Accordingly, Ni-NCM and Ni/Co-NCM show larger R_{ct} values compared to that of the pristine NCM while this value for Co-NCM and Ni&Co-NCM are comparable to the uncoated sample, and the smallest one belongs to Ni&Co-NCM. Hence, it can be concluded that $NiCo_2O_4$ is the most conducive coating to electrochemical impedance performance by optimizing the number of interfaces and the value of resistance in the coating layer.

For calculating the bulk modulus of materials, hydrostatic defor-

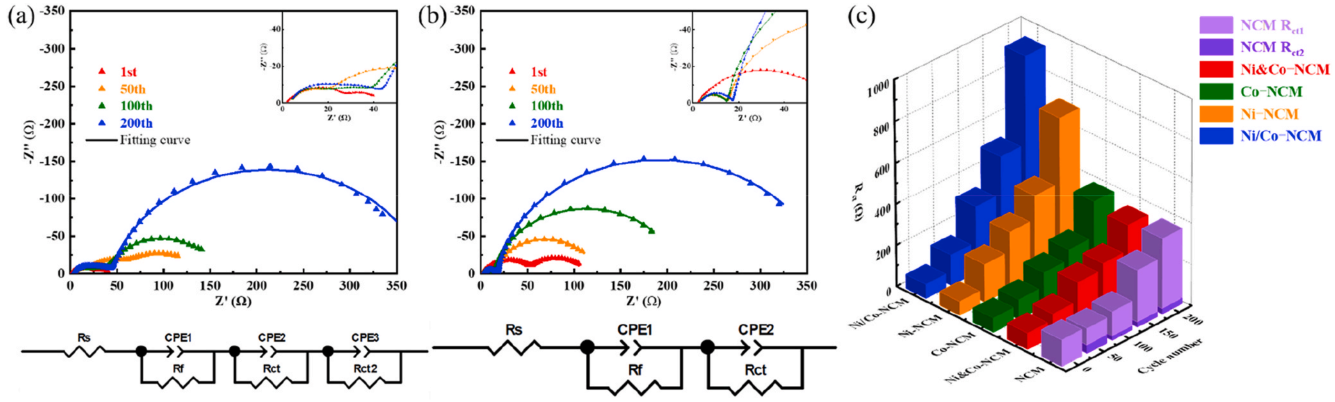

Fig. 5. Nyquist plots and fitting curves of (a) Pristine NCM and (b) Ni&Co-NCM; (c) Comparing the R_{ct} value for all samples.

mation was introduced into the optimized cell. The modulus was then predicted using Murnaghan equation of state [48], and according to this formula:

$$E(V) = E_0 + K_0 V_0 \left[\frac{1}{K_0^{'}\left(K_0^{'} - 1\right)} \left(\frac{V}{V_0} \right)^{1-K_0^{'}} + \frac{1}{K_0^{'}} \frac{V}{V_0} - \frac{1}{K_0^{'} - 1} \right]$$

The bulk modulus plots are demonstrated in Fig. 6b. It can be inferred that NiO (179.72 GPa) and $NiCo_2O_4$ (174.17 GPa) has similar bulk modulus while Co_3O_4 (165.97 GPa) is relatively softer due to the lower bulk modulus, which depends on the crystal structure and indicates that the strength of Ni–O bond is higher than that of Co–O bond. This characteristic signifies that NiO and $NiCo_2O_4$ have stronger inhibitory effect on the volume expansion and structural deterioration of the NCM during cycling compared to Co_3O_4 and its mixture with NiO.

Meanwhile, the calculated density of states is demonstrated in Fig. 6c. It can be realized that NiO is a wide bandgap semiconductor while both Co_3O_4 and $NiCo_2O_4$ turn out to be half metals. Such calculation indicates that $NiCo_2O_4$ has a much better electronic conductivity compared with NiO and a similar conductivity as Co_3O_4. Therefore, Co_3O_4 and $NiCo_2O_4$ coating layers hardly show resistance to electronic transmission, which also supports the EIS results (Fig. 5c) that $NiCo_2O_4$ and Co_3O_4 have a better electron conductivity than NiO and its mixture with Co_3O_4.

Considering the reaction of oxides (NiO, Co_3O_4 or $NiCo_2O_4$) with F^-, pseudo-binary phase diagram is constructed between the two ending compounds, so that the reaction energy at different ratios can be calculated. In order to get an accurate reaction energy, all possible reaction products were considered by enumeration of all ICSD compounds in the composition space of M (M = Ni or (and) Co)–O–H–F. The calculated reaction phase diagram between the oxides and F^- is presented in Fig. 6d. It can be inferred that NiO has a much lower formation energy compared with Co_3O_4 and $NiCo_2O_4$. Accordingly, it indicates that Co_3O_4 and $NiCo_2O_4$ are more effective in preventing NCM from reacting with F^- and consequently inhibiting the dissolution of active

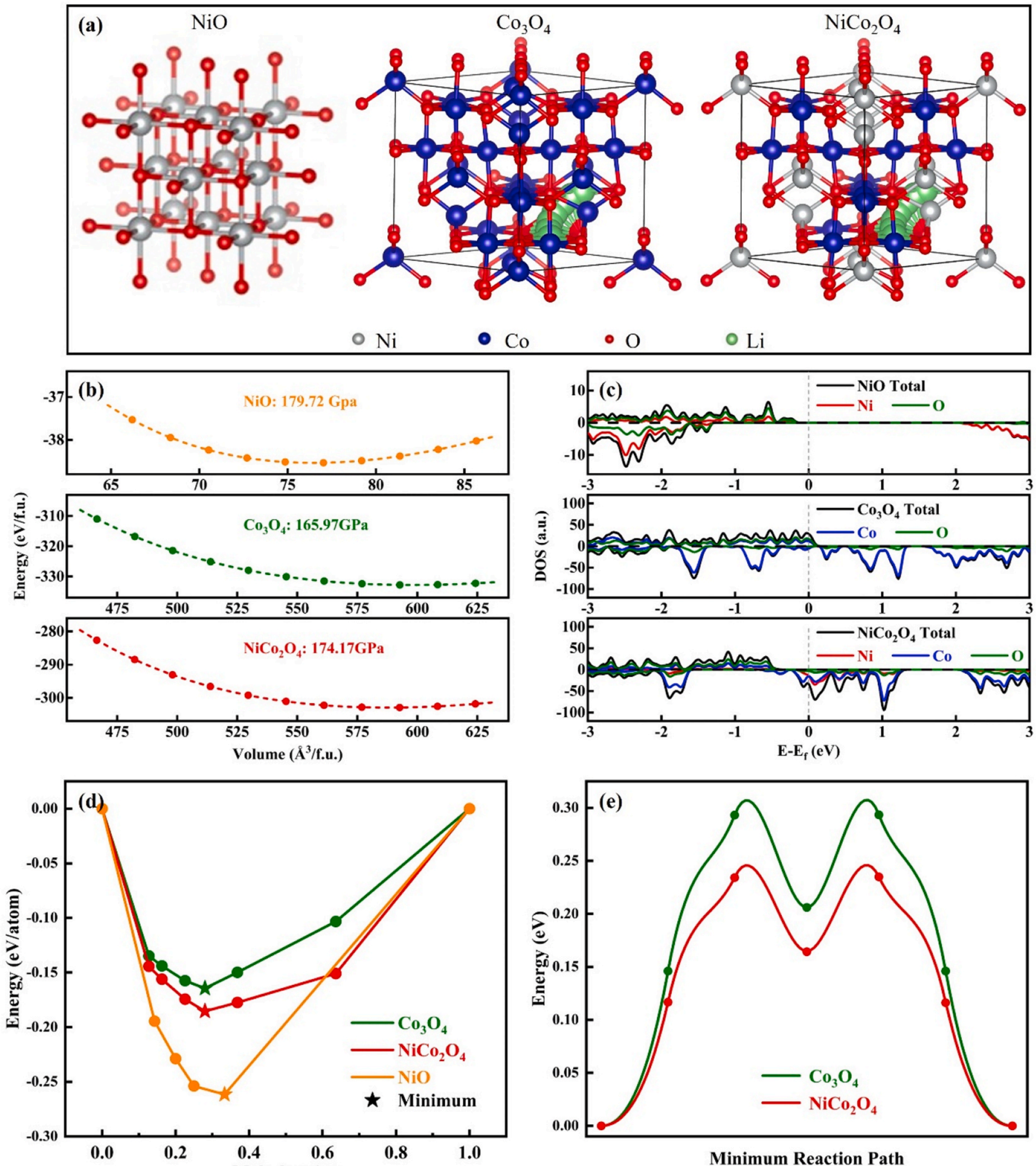

Fig. 6. (a) Crystal structure of NiO, Co_3O_4 and $NiCo_2O_4$, in which Co_3O_4 and $NiCo_2O_4$ have pathways for Li^+ diffusion; (b) Equation of state curve for three oxides and fitting bulk modulus; (c) Density of states (DOS) for three oxides; (d) Reaction phase diagrams of three oxides with F^-, in which the star indicates the composition with lowest formation energy; (e) Li^+ diffusion minimum reaction path in Co_3O_4 and $NiCo_2O_4$.

materials compared to NiO and its mixture with Co_3O_4. Moreover, it is worth noting that at the electrode interface of a real battery, the actual effective ratio between oxide and F^- is smaller since the oxide only serves as a coating material that is surrounded by electrolyte.

Regarding Li^+ migration in oxides, it should be noted that the rock-salt structure of NiO does not provide enough space to enable Li^+ diffusion. When it comes to Co_3O_4 and $NiCo_2O_4$ structure, the vacant octahedral site in spinel framework can easily allow Li^+ diffusion. It also verifies the lower value of ΔE_E for $NiCo_2O_4$ and Co_3O_4 compared to NiO, and is consistent with the results from Fig. 6d. To estimate the activation barrier, the climbing image Nudged Elastic Band (ci-NEB) method [33, 49–51] was adopted to compute the minimum reaction paths (MEPs) and the associated energy barriers of 2H/T phase transitions. Indeed, NEB calculations were only performed on Co_3O_4 and $NiCo_2O_4$, and the calculated MEPs are demonstrated in Fig. 6e. Additionally, the Li^+ diffusion barrier in $NiCo_2O_4$ is calculated to be around 234 meV, which is smaller than that of Co_3O_4, which is 293 meV. This result is in agreement with the CV results in Fig. 4d, and further validates the better ionic conductivity of $NiCo_2O_4$ relative to Co_3O_4.

To sum up, the bulk modulus of $NiCo_2O_4$ is superior to Co_3O_4, and compared to NiO, it has a less reaction with F^- and possesses a much better conductivity. Moreover, the activation barrier of $NiCo_2O_4$ is the lowest among the samples. According to the experimental and calculation results, $NiCo_2O_4$ exhibits the same structure as Co_3O_4 in terms of conducting Li^+, and addition of Ni increases the overall mechanical strength of the material. Indeed, the higher binding energy of Ni–O compared to Co–O bond together with the other constructive physical and chemical properties make $NiCo_2O_4$ superior to the other coating materials in terms of bulk modulus, stability against F-, electronic conductivity and Li^+ diffusion activation barrier, all of which can protect the cathode and stabilize its performance through cycling.

4. Conclusions

In this work, bimetallic oxide coatings on NCM811 were proved to have a superior performance over monometallic oxides which were used as the control groups. Specifically, as a result of the coatings, the electrochemical characteristics achieved different levels of improvement, among which the bimetallic oxide Ni&Co-NCM displayed the best performance. Ni&Co-NCM delivered a high initial CE of 82.92% and a high capacity retention of 90.97% after 200 cycles at 100 mA g^{-1}. Among the coatings, $NiCo_2O_4$ coating layer demonstrated the best elemental distribution, electrochemical stability and conductivity as well as the lowest charge transfer resistance owing to its electrochemically favorable crystal structure and more active elements. The theoretical calculations also confirmed that $NiCo_2O_4$ is the best coating material among the other candidates due to the superior bulk modulus, less reaction with F^-, better conductivity and lower activation barrier. $NiCo_2O_4$ has a similar structure as Co_3O_4 and exhibits better electrochemical properties than the rock-salt NiO in terms of the electronic and ionic conductivity. Moreover, the synergistic effect of nickel and cobalt is the primary reason for superiority of the bimetallic oxides compared to the monometallic oxides and their mixtures, where nickel atoms enhance the mechanical stability of the coating layer and cobalt atoms improve the diffusion rate of electrons and ions, which cannot be fully achieved in monometallic oxides. More importantly, this work has profound implications in the design of bimetallic and even polymetallic oxide coatings for electrode materials in the future. Nevertheless, not all bimetallic oxides can achieve a better performance than single metal oxides, thus evaluating the properties of single metal oxides prior to design a coating layer is essential. In future, a similar designing approach can be extended to more bimetallic coating materials such as sulfides and selenides.

Declaration of competing interest

This manuscript has not been published or presented elsewhere in part or in entirety and is not under consideration by another journal. All study participants provided informed consent, and the study design was approved by the appropriate ethics review boards. All the authors have approved the manuscript and agree with submission to your esteemed journal. There are no conflicts of interest to declare.

Acknowledgement

The authors gratefully acknowledge the financial support by the National Natural Science Foundation of China (51672189, 51772051 and 51801153), China Postdoctoral Science Foundation (2019M653705), Project 2019JPL-04 supported by Joint Foundation of Shaanxi, Natural Science Foundation of Shaanxi Province (2020JQ-638) and Xi'an Science and Technology Project of China (201805037YD15CG21(20)).

Appendix A. Supplementary data

Supplementary data to this article can be found online at https://doi.org/10.1016/j.nanoen.2020.105034.

References

[1] T.-H. Kim, J.-S. Park, S.K. Chang, S. Choi, J.H. Ryu, H.-K. Song, The current move of lithium ion batteries towards the next phase, Adv. Energy Mater. 2 (7) (2012) 860–872.

[2] N.S. Choi, Z. Chen, S.A. Freunberger, X. Ji, Y.K. Sun, K. Amine, G. Yushin, L. F. Nazar, J. Cho, P.G. Bruce, Challenges facing lithium batteries and electrical double-layer capacitors, Angew Chem. Int. Ed. Engl. 51 (40) (2012) 9994–10024.

[3] M. Li, J. Lu, Z. Chen, K. Amine, 30 Years of lithium-ion batteries, Adv. Mater. (2018), e1800561.

[4] W. Liu, P. Oh, X. Liu, M.J. Lee, W. Cho, S. Chae, Y. Kim, J. Cho, Nickel-rich layered lithium transition-metal oxide for high-energy lithium-ion batteries, Angew Chem. Int. Ed. Engl. 54 (15) (2015) 4440–4457.

[5] J.M. Lim, T. Hwang, D. Kim, M.S. Park, K. Cho, M. Cho, Intrinsic origins of crack generation in Ni-rich $LiNi_{0.8}Co_{0.1}Mn_{0.1}O_2$ layered oxide cathode, Mater. Sci. Rep. 7 (2017) 39669.

[6] F. Wu, N. Liu, L. Chen, Y. Su, G. Tan, L. Bao, Q. Zhang, Y. Lu, J. Wang, S. Chen, J. Tan, Improving the reversibility of the H2-H3 phase transitions for layered Ni-rich oxide cathode towards retarded structural transition and enhanced cycle stability, Nano Energy 59 (2019) 50–57.

[7] T. Weigel, F. Schipper, E.M. Erickson, F.A. Susai, B. Markovsky, D. Aurbach, Structural and electrochemical aspects of $LiNi_{0.8}Co_{0.1}Mn_{0.1}O_2$ cathode materials doped by various cations, ACS Energy Lett. 4 (2) (2019) 508–516.

[8] T. Li, X.-Z. Yuan, L. Zhang, D. Song, K. Shi, C. Bock, Degradation mechanisms and mitigation strategies of nickel-rich NMC-based lithium-ion batteries, Electrochem. Energy Rev. 3(1) (2020) 43–80.

[9] W. Li, U.H. Kim, A. Dolocan, Y.K. Sun, A. Manthiram, formation and inhibition of metallic lithium microstructures in lithium batteries driven by chemical crossover, ACS Nano 11 (6) (2017) 5853–5863.

[10] J. Li, H. Liu, J. Xia, A.R. Cameron, M. Nie, G.A. Botton, J.R. Dahn, The impact of electrolyte additives and upper cut-off voltage on the formation of a rocksalt surface layer in $LiNi_{0.8}Mn_{0.1}Co_{0.1}O_2$ electrodes, J. Electrochem. Soc. 164 (4) (2017) A655–A665.

[11] Y. Cho, P. Oh, J. Cho, A new type of protective surface layer for high-capacity Ni-based cathode materials: nanoscaled surface pillaring layer, Nano Lett. 13 (3) (2013) 1145–1152.

[12] F. Lin, D. Nordlund, Y. Li, M.K. Quan, L. Cheng, T.-C. Weng, Y. Liu, H.L. Xin, M. M. Doeff, Metal segregation in hierarchically structured cathode materials for high-energy lithium batteries, Nat. Energy 1 (1) (2016).

[13] H. Maleki Kheimeh Sari, X. Li, Controllable cathode–electrolyte interface of $Li[Ni_{0.8}Co_{0.1}Mn_{0.1}]O_2$ for lithium ion batteries: a review, Adv. Energy Mater. 9 (39) (2019) 1901597.

[14] K. Araki, N. Taguchi, H. Sakaebe, K. Tatsumi, Z. Ogumi, Electrochemical properties of $LiNi_{1/3}Co_{1/3}Mn_{1/3}O_2$ cathode material modified by coating with Al_2O_3 nanoparticles, J. Power Sources 269 (2014) 236–243.

[15] W. Zhu, X. Huang, T. Liu, Z. Xie, Y. Wang, K. Tian, L. Bu, H. Wang, L. Gao, J. Zhao, Ultrathin Al_2O_3 coating on $LiNi_{0.8}Co_{0.1}Mn_{0.1}O_2$ cathode material for enhanced cycleability at extended voltage ranges, Coatings 9 (2) (2019).

[16] K. Min, K. Park, S.Y. Park, S.-W. Seo, B. Choi, E. Cho, Residual Li reactive coating with Co3O4for superior electrochemical properties of $LiNi_{0.91}Co_{0.06}Mn_{0.03}O_2$ cathode material, J. Electrochem. Soc. 165 (2) (2018) A79–A85.

[17] F. Tao, X.-x. Yan, J.-J. Liu, H.-L. Zhang, L. Chen, Effects of PVP-assisted Co3O4 coating on the electrochemical and storage properties of $LiNi_{0.6}Co_{0.2}Mn_{0.2}O_2$ at high cut-off voltage, Electrochim. Acta 210 (2016) 548–556.

[18] W. Cho, S.-M. Kim, J.H. Song, T. Yim, S.-G. Woo, K.-W. Lee, J.-S. Kim, Y.-J. Kim, Improved electrochemical and thermal properties of nickel rich $LiNi_{0.6}Co_{0.2}Mn_{0.2}O_2$ cathode materials by SiO2 coating, J. Power Sources 282 (2015) 45–50.

[19] H. Kim, J. Jang, D. Byun, H.S. Kim, W. Choi, Selective TiO_2 nanolayer coating by polydopamine modification for highly stable nickel-rich layered oxides with 4.5 V high-voltage operation in rechargeable batteries, ChemSusChem 12 (2019).

[20] J.-Z. Kong, C. Ren, G.-A. Tai, X. Zhang, A.-D. Li, D. Wu, H. Li, F. Zhou, Ultrathin ZnO coating for improved electrochemical performance of $LiNi_{0.5}Co_{0.2}Mn_{0.3}O_2$ cathode material, J. Power Sources 266 (2014) 433–439.

[21] Z. Gan, G. Hu, Z. Peng, Y. Cao, H. Tong, K. Du, Surface modification of $LiNi_{0.8}Co_{0.1}Mn_{0.1}O_2$ by WO_3 as a cathode material for LIB, Appl. Surf. Sci. 481 (2019) 1228–1238.

[22] W. Cho, S.-M. Kim, K.-W. Lee, J.H. Song, Y.N. Jo, T. Yim, H. Kim, J.-S. Kim, Y.-J. Kim, Investigation of new manganese orthophosphate $Mn_3(PO_4)_2$ coating for nickel-rich $LiNi_{0.6}Co_{0.2}Mn_{0.2}O_2$ cathode and improvement of its thermal properties, Electrochim. Acta 198 (2016) 77–83.

[23] X. Xiong, Z. Wang, X. Yin, H. Guo, X. Li, A modified LiF coating process to enhance the electrochemical performance characteristics of $LiNi_{0.8}Co_{0.1}Mn_{0.1}O_2$ cathode materials, Mater. Lett. 110 (2013) 4–9.

[24] H. Yang, K. Wu, G. Hu, Z. Peng, Y. Cao, K. Du, Design and synthesis of double-functional polymer composite layer coating to enhance the electrochemical performance of the Ni-rich cathode at the upper cutoff voltage, ACS Appl. Mater. Interfaces 11 (8) (2019) 8556–8566.

[25] W. Liu, X. Li, D. Xiong, Y. Hao, J. Li, H. Kou, B. Yan, D. Li, S. Lu, A. Koo, K. Adair, X. Sun, Significantly improving cycling performance of cathodes in lithium ion batteries: the effect of Al_2O_3 and $LiAlO_2$ coatings on $LiNi_{0.6}Co_{0.2}Mn_{0.2}O_2$, Nano Energy 44 (2018) 111–120.

[26] J. Yang, Y. Xia, Suppressing the phase transition of the layered Ni-rich oxide cathode during high-voltage cycling by introducing low-content Li_2MnO_3, ACS Appl. Mater. Interfaces 8 (2) (2016) 1297–1308.

[27] R. Zhang, J. Wang, G. Yan, W. Peng, H. Guo, Z. Wang, X. Li, W. Gui, N. Chen, Enhancing the electrochemical and storage performance of Ni-based cathode materials by introducing spinel pillaring layer for lithium ion batteries, Solid State Ionics 332 (2019) 41–46.

[28] K. Meng, Z. Wang, H. Guo, X. Li, D. Wang, Improving the cycling performance of $LiNi_{0.8}Co_{0.1}Mn_{0.1}O_2$ by surface coating with Li_2TiO_3, Electrochim. Acta 211 (2016) 822–831.

[29] B. Song, W. Li, S.M. Oh, A. Manthiram, Long-life nickel-rich layered oxide cathodes with a uniform Li_2ZrO_3 surface coating for lithium-ion batteries, ACS Appl. Mater. Interfaces 9 (11) (2017) 9718–9725.

[30] X. Li, L. Jin, D. Song, H. Zhang, X. Shi, Z. Wang, L. Zhang, L. Zhu, $LiNbO_3$-coated $LiNi_{0.8}Co_{0.1}Mn_{0.1}O_2$ cathode with high discharge capacity and rate performance for all-solid-state lithium battery, J. Energy Chem. 40 (2020) 39–45.

[31] W. Yan, S. Yang, Y. Huang, Y. Yang, GuohuiYuan, A review on doping/coating of nickel-rich cathode materials for lithium-ion batteries, J. Alloys Compd. 819 (153048) (2019).

[32] W. Kohn, L.J. Sham, Self-consistent equations including exchange and correlation effects, Phys. Rev. 140 (4A) (1965) A1133–A1138.

[33] P. Hohenberg, W. Kohn, Inhomogeneous electron gas, Phys. Rev. 136 (3B) (1964) B864–B871.

[34] H. Xie, K. Du, G. Hu, J. Duan, Z. Peng, Z. Zhang, Y. Cao, Synthesis of $LiNi_{0.8}Co_{0.15}Al_{0.05}O_2$ with 5-sulfosalicylic acid as a chelating agent and its electrochemical properties, J. Mater. Chem. 3 (40) (2015) 20236–20243.

[35] W.Y. Li, L.N. Xu, J. Chen, Co3O4 nanomaterials in lithium-ion batteries and gas sensors, Adv. Funct. Mater. 15 (5) (2005) 851–857.

[36] G. Luo, K.S. Teh, Y. Xia, Z. Li, Y. Luo, L. Zhao, Z. Jiang, Construction of $NiCo_2O_4$@ NiFe LDHs core/shell nanowires array on carbon cloth for flexible, high-performance pseudocapacitor electrodes, J. Alloys Compd. 767 (2018) 1126–1132.

[37] C. Yuan, X. Zhang, L. Su, B. Gao, L. Shen, Facile synthesis and self-assembly of hierarchical porous NiO nano/micro spherical superstructures for high performance supercapacitors, J. Mater. Chem. 19 (32) (2009).

[38] M. Xu, Q. Xia, J. Yue, X. Zhu, Q. Guo, J. Zhu, H. Xia, Rambutan-like hybrid hollow spheres of carbon confined Co_3O_4 nanoparticles as advanced anode materials for sodium-ion batteries, Adv. Funct. Mater. 29 (6) (2018).

[39] Y. Su, Y. Yang, L. Chen, Y. Lu, L. Bao, G. Chen, Z. Yang, Q. Zhang, J. Wang, R. Chen, S. Chen, F. Wu, Improving the cycling stability of Ni-rich cathode materials by fabricating surface rock salt phase, Electrochim. Acta 292 (2018) 217–226.

[40] S. Gao, Y.T. Cheng, M. Shirpour, Effects of cobalt deficiency on nickel-rich layered $LiNi_{0.8}Co_{0.1}Mn_{0.1}O_2$ positive electrode materials for lithium-ion batteries, ACS Appl. Mater. Interfaces 11 (1) (2019) 982–989.

[41] X. Xu, H. Huo, J. Jian, L. Wang, H. Zhu, S. Xu, X. He, G. Yin, C. Du, X. Sun, Radially oriented single-crystal primary nanosheets enable ultrahigh rate and cycling properties of $LiNi_{0.8}Co_{0.1}Mn_{0.1}O_2$ cathode material for lithium-ion batteries, Adv. Energy Mater. 9 (15) (2019).

[42] C. Heubner, M. Schneider, A. Michaelis, Investigation of charge transfer kinetics of Li-Intercalation in $LiFePO_4$, J. Power Sources 288 (2015) 115–120.

[43] J.R. Dahn, J. Jiang, L.M. Moshurchak, M.D. Fleischauer, C. Buhrmester, L. J. Krause, High-rate overcharge protection of LiFePO[sub4]-Based Li-ion cells using the redox shuttle additive 2,5-Ditertbutyl-1,4-dimethoxybenzene, J. Electrochem. Soc. 152 (6) (2005).

[44] B. Yan, M. Li, X. Li, Z. Bai, J. Yang, D. Xiong, D. Li, Novel understanding of carbothermal reduction enhancing electronic and ionic conductivity of $Li_4Ti_5O_{12}$ anode, J. Mater. Chem. 3 (22) (2015) 11773–11781.

[45] Y. Wu, W. Wang, J. Ming, M. Li, L. Xie, X. He, J. Wang, S. Liang, Y. Wu, An exploration of new energy storage system: high energy density, high safety, and fast charging lithium ion battery, Adv. Funct. Mater. 29 (1) (2019).

[46] H.Q. Pham, E.H. Hwang, Y.G. Kwon, S.W. Song, Approaching the maximum capacity of nickel-rich $LiNi_{0.8}Co_{0.1}Mn_{0.1}O_2$ cathodes by charging to high-voltage in a non-flammable electrolyte of propylene carbonate and fluorinated linear carbonates, Chem. Commun. 55 (9) (2019) 1256–1258.

[47] Z. Yang, L. Bao, W. Li, L. Chen, Y. Su, Y. Lu, G. Chen, N. Liu, Q. Zhang, R. Chen, S. Chen, F. Wu, Synthesizing $LiNi_{0.8}Co_{0.1}Mn_{0.1}O_2$ with novel shell-pore structure for enhanced rate performance, J. Alloys Compd. 789 (2019) 736–743.

[48] C.L. Fu, K.M. Ho, First-principles calculation of the equilibrium ground-state properties of transition metals: applications to Nb and Mo, Phys. Rev. B 28 (10) (1983) 5480–5486.

[49] D. Sheppard, R. Terrell, G. Henkelman, Optimization methods for finding minimum energy paths, J. Chem. Phys. 128 (13) (2008) 134106.

[50] G. Henkelman, B.P. Uberuaga, H. Jónsson, A climbing image nudged elastic band method for finding saddle points and minimum energy paths, J. Chem. Phys. 113 (22) (2000) 9901–9904.

[51] R.A. Olsen, G.J. Kroes, G. Henkelman, A. Arnaldsson, H. Jonsson, Comparison of methods for finding saddle points without knowledge of the final states, J. Chem. Phys. 121 (20) (2004) 9776–9792.

Quan Xu is currently a graduate student in the Institute of Advanced Electrochemical Energy at Xi'an University of Technology. He received B.S. degree in School of Materials Science and Engineering, Xi'an University of Technology in 2016. His research interests focus on the modification and application of cathode materials for lithium ion batteries.

Xifei Li is currently a full professor at Xi'an University of Technology, and a fellow of Royal Society of Chemistry. He was awarded as 2018 & 2019 Highly Cited Researchers of Clarivate Analytics. He is an executive editor-in chief of Electrochemical Energy Reviews, a vice-president of International Academy of Electrochemical Energy Science, and a vice-director of Full Cell Engine Sub-society of Chinese Society of Internal Combustion Engines. Dr. Li's research group is working on optimized interfaces of the anodes and the cathodes with various structures for high performance rechargeable batteries. Dr. Li has authored/ co-authored 230 articles with 12000 citations.

Hirbod Maleki Kheimeh Sari is currently a Ph.D. candidate in the Institute of Advanced Electrochemical Energy at Xi'an University of Technology. He received his Master's degree from the College of Mechanical Engineering, Malaysia University of Technology in 2014. His research interests primarily focus on the design and synthesis of novel nanomaterials for energy storage, especially cathode materials for lithium/sodium ion batteries.

Wenbin Li received his B.S., M.S. and Ph.D. in School of Materials Science & Engineering from Shaanxi University of Science & Technology in 2013, 2016 and 2019, respectively. Now he is a lecturer in Institute of Advanced Electrochemical Energy & School of Materials Science and Engineering from Xi'an University of Technology. His current research interests focus on energy storage materials and devices.

Wen Liu received his B.S. degree from College of Chemistry and Materials Science, Shanxi normal University in 2015. He is a Ph. D. candidate of Xi'an Key Laboratory of New Energy Materials and Devices, Institute of Advanced Electrochemical Energy & School of Materials Science and Engineering, Xi'an University of Technology. His research is focus on the interfacial design, synthesis and structural characterization of Ni-rich cathode materials for high performance Lithium ion batteries.

Youchen Hao is a PhD student at Xi'an university of Technology. His research interests focus on electrochemical energy storage, especially the design and synthesis of cathode materials for Li-ion and Li–S batteries.

Jian Qin is an associate professor at school of material science and engineering of Xi'an University of Technology (China). Prior to joining XAUT in 2018, he completed his Ph.D in material science at Tianjin University (China). His current research focused on nanostructure design, fabrication and properties for energy and environment application, including sodium-ion battery and potassium-ion battery.

Bin Cao received his bachelor degree from Xi'an University of Science and Technology in 2012 and Ph.D. degree from Beijing University of Chemical Technology in 2018 under the guidance of Prof. Huaihe Song. His research interests focused on carbon materials science and engineering, especially in new carbon-based materials for eletrochemical energy storage/conversion.

Wei Xiao is currently a postdoctoral fellow at Xi'an University of Technology in China. He received his bachelor degree in 2010 and master degree in 2013 from Central South University (China). Later, he achieved his Ph.D. degree from University of Western Ontario (Canada) under the supervision of Prof. Xueliang (Andy) Sun and Prof. Tsun-Kong Sham in 2017. His research interests focus on the development of high-performance anode materials for sodium/potassium-ion batteries. His current research works are also related to synchrotron-based X-ray characterizations on energy materials.

Yue Xu received her B.D. degree in School of Material Physics, Xi'an University of Technology in 2017. Her research is focus on the design and synthesis of novel nanomaterial for energy storage, especially cathode materials for lithium/sodium ion batteries.

Yuan Wei is currently a graduate student in the College of Materials Science and Engineering, Xi'an University of Technology. She received her B.D. degree in School of Materials Science and Engineering, Xi'an University of Technology in 2017.Her research interests focus on the design and application of cathode materials for lithium ion batteries.

Liang Kou received his Ph.D. degree in 2014 from Polymer Chemistry and Physics at Zhejiang University under the direction of Prof. Chao Gao. Now he is a research scientist in Shaanxi Coal and Chemical Technology Institute Co., Ltd. His research interests focus on the synthesis and mass production of cathode, anode materials for lithium batteries.

Zhan Yuan Tian is a researcher of New Energy Technology Department, Shaanxi Coal and Chemical Technology Institute Co., Ltd. And he is currently studying for a PhD degree from Xi'an Jiaotong University. He received his Master of Engineering degree from Zhejiang University in 2010. His research interests focus on the negative and positive materials and the rational design for lithium ion batteries.

Le Shao is a researcher of New Energy Technology Department, Shaanxi Coal and Chemical Technology Institute Co., Ltd. He received his PhD degree from Shanghai Institute of Ceramics, Chinese Academy of Sciences in 2013. He works on the design and manufacturing for lithium ion batteries.

Cheng Zhang is an engineer in Shaanxi Coal Chemical Technology Research Institute Co. Ltd. He received his Master degree from Central South University in 2013. His main research interest is focused on the synthesis of lithium nickel cobalt manganese/aluminum oxides cathode materials and their battery application in electric vehicles and portable devices

Professor Xueliang Sun is a Senior Canada Research Chair (Tier 1) and Full Professor at the University of Western Ontario, Canada. Dr Sun received his Ph.D. in 1999 at the University of Manchester, UK, which he followed up by working as a postdoctoral fellow at the University of British Columbia, Canada and as a Research Associate at 1′Institut national de la recherche scientifique (INRS), Canada. His current research interests are associated with advanced materials for electrochemical energy storage and conversion, including electrocatalysis and catalyst support in fuel cells and electrodes in lithium-ion batteries and metal-air batteries.